SLAC-PUB-15922

APS/123-QED

Observations of continuum depression in warm dense matter with x-ray Thomson scattering

L. B. Fletcher,[1,2] A. L. Kritcher,[3] A. Pak,[3] T. Ma,[3] T. Döppner,[3] C. Fortmann,[3] L. Divol,[3] O. S. Jones,[3] O.L.Landen,[3] H. A. Scott,[3] J. Vorberger,[4] D. A. Chapman,[5,6] D. O. Gericke,[6] B. Mattern,[7] G. T. Seidler,[7] G. Gregori,[8] R. W. Falcone,[2] and S. H. Glenzer[1]

[1]*SLAC National Accelerator Laboratory, 2575 Sand Hill Road, MS 72 Menlo Park, CA 94025 USA*
[2]*Physics Department, University of California, Berkeley, California 94720, USA*
[3]*L-399, Lawrence Livermore National Laboratory, University of California, P.O. Box 808, Livermore, CA 94551, USA*
[4]*Max-Planck-Institut für die Physik komplexer Systeme, 01187 Dresden, Germany*
[5]*Plasma Physics Group, AWE plc, Aldermaston, Reading RG7 4PR, UK*
[6]*Centre for Fusion, Space and Astrophysics, Department of Physics, University of Warwick, Coventry CV4 7AL, United Kingdom*
[7]*Physics Department, University of Washington*
[8]*University of Oxford, Parks Road, Oxford, OX1 3PU, UK*

(Dated: February 27, 2014)

Detailed measurements of the electron densities, temperatures, and ionization states of compressed CH shells approaching pressures of 50 MBar have been achieved with spectrally resolved x-ray scattering. Laser-produced 9 keV x-rays probe the plasma during the transient state of three-shock-coalescence. High signal-to-noise x-ray scattering spectra show direct evidence of continuum depression in highly degenerate warm dense matter states with electron densities $n_e > 10^{24}\text{cm}^{-3}$. The measured densities and temperatures agree well with radiation-hydrodynamic modeling when accounting for continuum lowering in calculations that employ detailed configuration accounting.

PACS numbers: 52.25.Os, 52.35.Fp, 52.50.Jm, 78.70.Ck

Accurate knowledge of the ionization balance, the thermodynamic properties, and the equation of state of dense plasmas are of fundamental importance towards precisely modeling Warm Dense Matter (WDM) and materials in the High-Energy Density (HED) physics regime. Such information is relevant for understanding matter at Mbar pressures and temperatures beyond 1 eV that are predicted to exist in many astrophysical environments, interiors of giant planets [1–5], and occur during the thermonuclear fuel assembly phase of inertial confinement fusion implosions [6, 7]. As experiments are currently taking place at the National Ignition Facility (NIF) that achieve laser-driven compressed matter densities of up to 1000 g cm^{-3} [8–10], accurate plasma models are needed as an integral part of the experimental design [11, 12] of ignition conditions. Thus, it is important to experimentally characterize highly compressed states of matter in order to determine the physical properties and to evaluate current state–of–the–art radiation-hydrodynamic modeling.

HED conditions are produced via the interaction of high-power lasers with solid density targets [13]. Modern laser pulse shaping techniques drive multiple, precisely time-delayed shock waves. These separate shocks, controlled by the laser intensity and pulse duration, coalesce inside the solid and compress the material to high electron densities, $n_e > 10^{24}\text{cm}^{-3}$. achieving high pressures that approach, $P \simeq 50$ Mbar, at fairly low electron temperatures, thus resulting in nearly-degenerate strongly-coupled plasmas characterized by $T_e < T_F$ and $\Gamma_{ii} > 1$. Here, $T_F = \frac{\hbar^2}{2m_e}\left(3\pi^2 n_e\right)^{2/3}$ is the Fermi energy and Γ_{ii} is defined as the ratio of the Coulomb energy and the thermal energy. The theoretical description of these conditions is very challenging as standard solid-state theories and plasma expansion techniques do not apply. In addition, the experimental investigation of these states are equally challenging because these plasmas are not self emitting and require active probing by high-power penetrating x-rays or particle beams.

X-ray Thomson scattering has proven to be an accurate method to measure the electron density and temperature of highly compressed dense plasmas [13–31]. This technique probes the bulk properties of matter deep inside dense plasmas and is not limited by refraction and reflection at the surface boundary. In the non-collective scattering regime, the width of the inelastic Compton scattering distribution is a sensitive function of the momentum distribution of free or weakly bound electrons.

When the ionization state is known, the Compton scattering width has been applied to infer the electron density while the spectral shape is sensitive to the electron temperature [31–33]. The relative strength of the elastic scattering, in contrast, is sensitive to the ion temperature and is weakly correlated with the electron density. Consequently, high-signal-to noise measurements of both the elastic and inelastic scattered signals provide simultaneously the temperature and the electron density from a single scattering spectrum.

In this letter, we present the first measurements of continuum depression [34–37] in well-characterized compressed matter from spectrally resolved x-ray Thomson scattering (XRTS). The spectrum indicates the absence

Submitted to American Physical Society.

Division of Materials Sciences and Engineering, under contract DE-AC02-76SF00515 and BES.

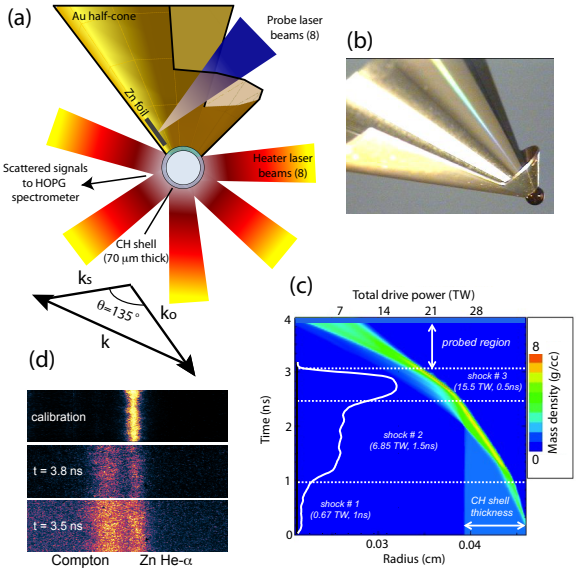

FIG. 1. (Color) The experimental setup to study spherically coalescing shocks in CH capsules is shown; a.) Schematic diagram of the target geometry, laser beam configuration, and scattering k-vectors; b.) Photograph of CH cone- in-half-shell target; c.) Radiation hydrodynamic simulation of the mass density is shown as a function of CH shell radius, the input laser drive power is superimposed as a white curve; d.) Raw x-ray scattering data measured with gated HOPG crystal spectrometer: calibration shot, measuring the Zn He$-\alpha$ line at 9 keV; scattered x-ray signals for 800 ps and 500 ps after end of the laser drive show elastic and Compton scattering features.

of valence carbon L-shell electrons that are highly localized in momentum space and provide a narrow spectral band signature. These findings were enabled by applying the full multi-ion species from factor in random phase approximation to determine the elastic scattering feature and the temperature. Thus, different from previous studies in CH [31, 33], both the elastic and inelastic XRTS features have been described for the first time providing the ionization state with high accuracy.

Our results demonstrate high values of the carbon ionization state Z_C after shock coalescence, that are in agreement with the hydrodynamic models that use Detailed Configuration Accounting (DCA), the Livermore Equation of State (LEOS) and incorporate the Stewart-Pyatt (SP) model [38] to calculate continuum depression. As a direct result, the calculated electron density is significantly larger than obtained with more widely used radiation-hydrodynamic orbital-free simulations that can employ selective equation of state tables and an ion-sphere (IS) model [39].

Figure (1) shows a schematic of the experimental configuration and the target geometry. This pump-probe experiment, performed at the Laboratory for Laser Energetics Omega Laser Facility [40], uses 70μm thick CH shells that are shock-compressed up to 8.75 g/cc using a pulse shape composed of three steps of 1 ns, 1.5 ns, and 500 ps duration along with precisely controlled total amplitudes of 0.67 TW, 6.85 TW, and 15.5 TW respectively. A total of 45 3ω (351 nm) laser beams, 13.5 kJ at 300 J/beam are focused to 800μm diameter spots and distributed over 75 % of the capsule surface area excluding the scattering line-of-sight cone as shown in Figs. (1d) and (1b). A total of eight laser beams produce high-energy Zn He$-\alpha$ x-rays at 9 keV. The x-ray probe is delayed by approximately 200 ps to 800 ps after the time of full shock coalescence probing the plasma at a scattering angle of $\theta = 135^\circ \pm 10^\circ$.

The laser pulse intensity profile is shown in Figure (1d) superimposed on a result from Helios 1-D radiation-hydrodynamic simulations [41], of the shell mass density as function of time and shell radius. The simulations demonstrate three shock coalescence at the end of the 3 ns drive and 50μm behind the inner shell boundary indicating peak mass density of $\rho = 8\rho_0$ at a temperature of $T_e = 17$ eV. The scattered signals from the shock compressed CH shell have been spectrally and temporally resolved with a graphite crystal (highly-oriented pyrolytic graphite) in combination with a gated microchannel plate detector capable of providing temporal resolution of 200 ps. Figure 1d shows sample x-ray scattering raw data from this configuration.

Figure (2) shows the scattering spectra at four different times after shock coalescence. The data are background subtracted and the x-ray filter and detector response has been taken into account. The x-ray energy and scattering angle results in non-collective scattering where the Compton scattering spectrum from free electrons yields a Compton shift of $E_C = \hbar^2 k^2/2m_e = 245$ eV.

The full spectral x-ray scattering response for a multi-component species can be described by the total electron structure factor, which allows the following decomposition [42]

$$S_{ee}^{tot}(\omega) = \sum_{a,b} \sqrt{x_a x_b}\, |f_a + q_a|\, |f_b + q_b|\, S_{ab}(\omega) + \widetilde{Z} S_{ee}^{0}(\omega) + \sum_a Z_a^c x_a \int d\omega' \widetilde{S}_a^{ce}(\omega - \omega') S_a^S(\omega') \; . \quad (1)$$

Here, f is the ion form factor, q describes the screening cloud, S_{ab} is the partial structure factor and $S_{ee}^0(\omega)$ is the full dynamic response of the free electrons in the system. The first term contains the resonant quasi-elastic Rayleigh scattering feature from tightly bound and screening electrons associated to different ion species, the second term describes Compton scattering from free electrons, while the third term contains the bound-free scattering contribution [13, 43–45].

In our conditions, we are probing the plasma in a finite$-\mathbf{k}$ regime where it is important to treat the electrons with the full random phase approximation for arbitrary $\mathbf{k}$ [46]. This procedure provides an accurate model for the elastic Rayleigh scattering contribution in multiple ion species [42] where the Rayleigh amplitude pro-

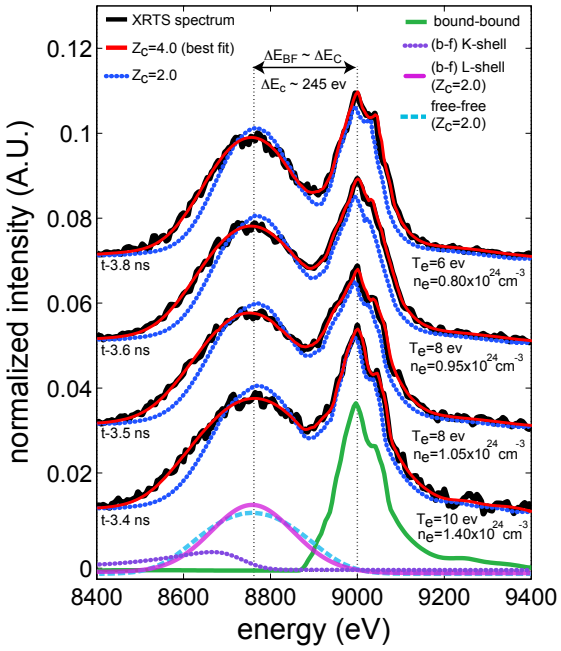

FIG. 2. (Color) Top spectra: X-ray Thomson scattering data and curve fit analysis. Measured scattering spectra (black data) and best fit (red curves) to the elastic and inelastic x-ray scattering from three-shocked CH capsules at t = 3.4 ns, 3.5 ns, 3.6 ns, and 3.8 ns, yield n_e, T_e, and carbon ionization state Z_C. The total best fit calculated x-ray scattering spectra for $Z_C = 4$ (red curves) are also compared to calculated spectra with $Z_C = 2$ (dark blue curves), and individual scattering features using the Impulse Approximation with the Dirac-Fock 2s wave function for the L-shell bound-free contribution (light purple curve), the core K-shell contribution (dark purple curve), the free-free Compton scattering contribution (light blue curve), and the elastic x-ray bound-bound scattering contribution (dark green).

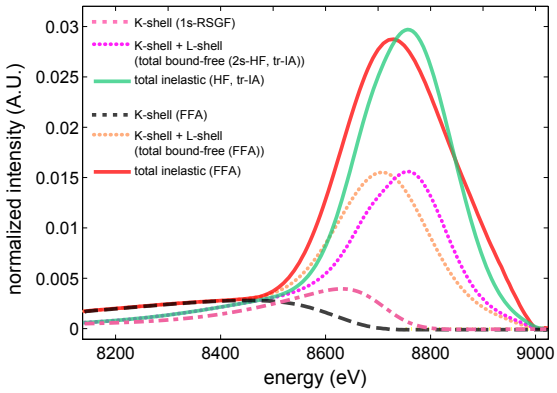

FIG. 3. (Color online) - Theoretical total inelastic bound-free x-ray scattering spectra using the truncated IA (green, tr-IA) and the FFA (red). Also shown are the separate contributions from K- and L-shell electrons within each approximation. The dashed red curve for the K-shell contribution uses the Real Space Green's Function (RSGF) approach

vides the temperature of the plasma and consequently constraints the fit of the inelastic feature. [47–50].

In addition, the bound-free scattering contribution depends on the average ionization state of the plasma for both carbon and hydrogen. For warm dense matter conditions explored here, the hydrogen atoms are fully ionized ($Z_H = 1$), but carbon ions provide a bound-free scattering component that yields the ionization state of the compressed CH capsule. In this study, the atomic L-shell contribution was calculated in the Impulse Approximation (IA) [51] from the Hartree-Fock (HF) 2s wave function [52] as suggested to provide accurate results by a recent study in Ref. [53].

For a carbon ionization state of $Z_C = 4$ we obtain an excellent fit to the inelastic Compton scattering spectrum. In particular, the width and spectral shape of the Compton scattering spectrum is properly described, cf. Fig. (2). On the other hand, when assuming a carbon charge state of $Z_C = 2$ the spectral fit calculations in the IA show significant discrepancies to the measured inelastic scattering spectrum. This is due to the narrow momentum distribution of L-shell electrons; for $Z_C = 2$ the intensity and spectral width of the L-shell spectrum is determined by the f-sum rules and the bound electron wave function, respectively, and consequently varying plasma density and temperature can not compensate for these properties.

We find that this result is independent of bound-free models used in Eq. (1), Figure (3) compares results obtained in IA with those obtained in the Form Factor Approximation (FFA). Although applying FFA results in some improvements on the low-energy wing of the inelastic scattering spectrum the FFA bound-free spectrum falls short in providing a good description of the data in the range 8800 eV$< E <$ 8900 eV, i.e., between the elastic and inelastic scattering contributions.

The supporting documents show attempts to fit the experimental data for a carbon ionization state of $Z_C = 2$ using FFA and with a different wave function model in IA [54]. In addition, we show a comparison with fits using $Z_C = 3$. These results demonstrate that good agreement between spectral fit calculations and experimental data can only be obtained using a carbon charge state of $Z_C = 4$ indicating the ionization of the carbon L-shell electrons in compressed CH. With this result at hand, the spectral shape of the inelastic Compton scattering spectrum further determines the temperature of free electrons [13, 32] providing results that match the temperature inferred from the elastic Rayleigh scattering amplitude. Thus, we estimate that the errors bars are less than 10 % in the measured electron density and 15 % in temperature and 0.5 for the ionization state Z.

Figure (4) compares the measured densities and temperature data during shock coalescence with the predicted values based on radiation-hydrodynamic simulations [56]. Four different conditions have been studied, and the scattering spectra have been analyzed using IA

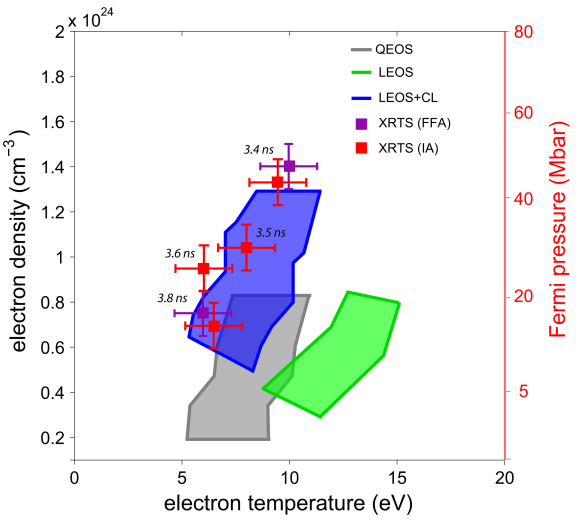

FIG. 4. (Color online) - Electron density vs temperature data inferred from spectrally resolved x-ray Thomson scattering (using bound-free models IA (red) and FFA (purple)). Green, grey, and blue regimes are from radiation-hydrodynamic simulations of multi-shocked compressed CH capsules incorporating various equation of state and continuum lowering models. Also shown is the Fermi pressure achieved in these experiments.

and FFA for the bound-free scattering contributions. For the lowest and highest pressure cases, we find slight differences using FFA vs IA due to slight differences in the calculated K-shell bound-free spectrum as indicated in Fig. (3). However, the differences are small and within the range of error bars and indicate Fermi pressures of 50 Mbar.

The experimental data are compared to three different radiation-hydrodynamic simulations. We obtain agreement using the LEOS, and include continuum lowering by the SP model through DCA. This contrast to modeling that uses various EOS modeling, but that neglects the shell structure of the ions as demonstrated by the LEOS or the quotidian EOS [57] calculations. These results demonstrate that simulations that include continuum lowering models agree with the data. In particular, the free electron density achieved in this experiment is about a factor of two larger than predicted by orbital-free modeling.

The study of ionization balance, as a consequence of ionization potential depression (IPD) in dense plasmas, has gained considerable interest recently with the ability to accurately monitor continuum edge shifts using narrow-band hard x-ray sources [36]. Those studies have primarily focused on continuum depression using K$-\alpha$ emission spectra from x-ray heated ($70 < T_e < 180$ eV), solid-density aluminum. Another recent study on hot compressed matter [37] has reported the lack of the Lyman$-\beta$ emission lines for densities larger than $\rho >$ 5.5 g/cc indicating that the SP model [38] appears to be in better agreement than the IPD model put forth by Ecker and Kröll (EK) [58]. In highly compressed nearly Fermi-degenerate warm dense matter studied here, there are no significant differences between these two models. The present results show IPD effect in shock-compressed warm dense matter and demonstrate the importance of including IPD effects in radiation-hydrodynamic modeling.

In conclusion, high signal-to-noise measurements and sensitivity of the carbon L-shell bound-free scattering spectra have accurately determined a carbon charge state of $Z_C = 4$, at pressures of approaching 50 Mbar, resulting in approximately two times higher free electron density than standard radiation-hydrodynamic modeling. Such higher than predicted ionization is consistent with conclusion from recent experiments performed at the Linac Coherent Light Source [36], and furthermore demonstrates the utility of material compression experiments to evaluate IPD models. These results have important implications for inertial confinement fusion studies where knowledge of the electron density in shock-compressed warm dense matter affects the calculation of hydrodynamic instabilities in the design of capsule implosion experiments.

This work was performed by the assistance of Lawrence Livermore National Laboratory (LLNL) under Contract DE-AC52-07NA27344 and supported by Laboratory Directed Research and Development (LDRD) grant 11-ER-050. This work was partially supported by the DOE Office of Science, Fusion Energy Sciences under FWP 100182 and y DOE Office of Basic Energy Sciences, Materials Sciences and Engineering Division, under Contract DE-AC02-76SF00515. Acknowledgements also extend to financial support by National Laser User Facility (NLUF) Grants: DE-FG52-07 NA28057 & DE-DE-FG52-09 NA29035 and to partial funding by UK EPSRC grant EP/G007187/1.

[1] T. Guillot, Science **286**, 72 (1999).
[2] G. W. Collins *et al.*, Phys. Rev. Lett. **87**, 165504 (2001).
[3] H. M. Van Horn, Science **252**, 384 (1991).
[4] M. D. Knudsen *et al.*, Phys. Rev. Lett. **108**, 091102 (2012).
[5] M Koenig *et al.*, Plasma Phys. Contr. Fusion **47**, B441 (2005).
[6] J. D. Lindl *et al.*, Phys. Plasmas **11**, 339 (2004).
[7] .S. Atzeni and J. Meyer-ter-Vehn, The Physics of Inertial Fusion (Clarendon Press, Oxford, 2004).
[8] H. F. Robey *et al.*, Phys. Rev. Lett. **108**, 215004 (2012).
[9] A. J. Mackinnon *et al.*, Phys. Rev. Lett. **108**, 215005 (2012).
[10] S. H. Glenzer *et al.*, Phys. Plasmas **19**, 056318 (2012).
[11] M. J. Edwards *et al.*, Phys. Plasmas **18**, 051003 (2011).
[12] S. W. Haan et al., Phys. Plasmas **18**, 051001 (2011).

[13] S. H. Glenzer and R. Redmer, Rev. Mod. Phys. **81**, 1625 (2009).
[14] S. H. Glenzer *et al.*, Phys. Rev. Lett. **90**, 175002 (2003).
[15] G. Gregori *et al.*, Phys. Plasmas **11**, 2754 (2004).
[16] G. Gregori *et al.*, J. Quant. Spectrosc. Radiat. Transfer, **99**, 225 (2006).
[17] H. Sawada *et al.*, Phys. Plasmas **14**, 122703 (2007).
[18] S. H. Glenzer *et al.*, Phys. Rev. Lett. **98**, 065002 (2007).
[19] A. L. Kritcher *et al.*, Science, **322**, 69 (2008).
[20] E. Garcia Saiz *et al.*, Nature Phys., **4**, 940 (2008).
[21] G. Gregori *et al.*, Phys. Rev. Lett. **101**, 045003 (2008).
[22] B. Barbrel *et al.*, Phys. Rev. Lett. **102**, 165004 (2009).
[23] H.-J. Lee *et al.*, Phys. Rev. Lett. **102**, 115001 (2009).
[24] A. L. Kritcher *et al.*, Phys. Rev. Lett. **103**, 245004 (2009).
[25] P. Neumayer *et al.*, Phys. Rev. Lett. **105**, 075003 (2010).
[26] A. Pelka *et al.*, Phys. Rev. Lett. **105**, 265701 (2010).
[27] C. Fortmann *et al.*, Phys. Rev. Lett. **108**, 175006 (2012).
[28] A. Visco *et al.*, Phys. Rev. Lett. **108**, 145001 (2012).
[29] S. Regan *et al.*, Phys. Rev. Lett. **109**, 265003 (2012).
[30] T. Ma *et al.*, Phys. Rev. Lett. **110**, 065001 (2013).
[31] A. L. Kritcher *et al.*, Phys. Rev. Lett. **107**, 015002 (2011).
[32] O. L. Landen *et al.*, J. Quant. Spectrosc. Radiat. Transfer, **71**, 465 (2001).
[33] L. B. Fletcher, *et al.*, Phys. Plasmas **20**, 056316 (2013).
[34] H. R. Griem, *Principles of Plasma Spectroscopy* (Cambridge University Press, Cambridge, England 1997).
[35] R. P. Drake, *High-Energy-Density Physics* (Springer, Berlin, Germany 2006).
[36] O. Ciricosta *et al.*, Phys. Rev. Lett. **109**, 065002 (2012).
[37] D. J. Hoarty *et al.*, Phys. Rev. Lett. **110**, 265003 (2013).
[38] J. C. Stewart and K. D. Pyatt, Jr., Astrophys. J. **144**, 1203 (1966).
[39] R. M. More, J. Quant. Spectrosc. Radiat. Transfer **27**, 345 (1982).
[40] J. M. Soures *et al.*, Fusion Technology, **30**, 492 (1996).
[41] J. MacFarlane, et al., J. Quant. Spectrosc. Radiat. Transf. **99**, 381 (2006).
[42] K. Wünsch *et al.*, Europ. Phys. Letters, **94** 25001 (2011).
[43] J. Chihara, J. Phys.: Condens. Matter, **12**, 231 (2000).
[44] G. Gregori *et al.*, Phys. Rev. E **67**, 026412 (2003).
[45] G. Gregori *et al.*, Phys. Rev. E **74**, 026402 (2006).
[46] D. A. Chapman *et al.*, Phys. Rev. Letters, *to be submitted*, (2013).
[47] D. O. Gericke *et al.*, Phys. Rev. E **81**, 065401(R) (2010).
[48] N. R. Arista and W. Bandt, Phys. Rev. A **29**, 1471 (1984).
[49] D. Pines, and D. Bohm, Phys. Rev. **85**, 338 (1952).
[50] D. Pines, and P. Nozieres, *The Theory of Quantum Fluids* (Addison-Wesley, Redwood, CA, 1990).
[51] P. Eisenberger and P. M. Platzman, Phys. Rev. A **2**, 415 (1970).
[52] A.L. Ankudinov, S. I. Zabinskyb, and J. J. Rehra, Computer Phys. Comm. **98** 359 (1996).
[53] B. A. Mattern and G. T. Seidler, Phys. Plasmas **20**, 022706 (2013).
[54] See supplementary material at http://link.aps.org, which includes Ref. [55].
[55] I Golovkin et al. *et al.*, High Energy Density Physics **9**, 510 (2013).
[56] M. M. Marinak *et al.*, Phys. Plasmas **8**, 2275 (2001).
[57] R. M. More *et al.*, Phys. Fluids **31**, 3059 (1988).
[58] G. Ecker and W. Kröll, Phys. Fluids 6, 62 (1963).